

Visible-to-mid-IR tunable frequency comb in nanophotonics

Arkadev Roy^{1*}, Luis Ledezma^{1,2*}, Luis Costa¹, Robert Gray¹, Ryoto Sekine¹,

Qiushi Guo¹, Mingchen Liu¹, Ryan M. Briggs², and Alireza Marandi^{1†}

¹Department of Electrical Engineering, California Institute of Technology, Pasadena, California 91125, USA

²Jet Propulsion Laboratory, California Institute of Technology, Pasadena, California 91109, USA

* These authors contributed equally to this work and

†marandi@caltech.edu

Optical frequency comb is an enabling technology for a multitude of applications from metrology to ranging and communications. The tremendous progress in sources of optical frequency combs has mostly been centered around the near-infrared spectral region while many applications demand sources in the visible and mid-infrared, which have so far been challenging to achieve, especially in nanophotonics. Here, we report frequency combs tunable from visible to mid-infrared on a single chip based on ultra-widely tunable optical parametric oscillators in lithium niobate nanophotonics. Using picosecond-long pump pulses around $1\ \mu\text{m}$ and tuning of the quasi-phase matching, we show sub-picosecond frequency combs tunable beyond an octave extending from $1.5\ \mu\text{m}$ up to $3.3\ \mu\text{m}$ with femtojoule-level thresholds. We utilize the up-conversion of the infrared combs to generate visible frequency combs reaching $620\ \text{nm}$ on the same chip. The ultra-broadband tunability and visible-to-mid-infrared spectral coverage of our nanophotonic source can be combined with an on-chip picosecond source as its pump, as well as pulse shortening and spectral broadening mechanisms at its output, all of which are readily available in lithium niobate nanophotonics. Our results highlight a practical and universal path for realization of efficient frequency comb sources in nanophotonics overcoming their spectral sparsity.

Optical frequency combs consisting of several spectral lines with accurate frequencies are at the core of a plethora of modern-day applications [1, 2], including spectroscopy [3], optical communication [4], optical computing [5], atomic clocks [6], ranging [7, 8] and imaging [9]. Many of these applications demand optical frequency combs in the technologically important mid-infrared [10, 11] and visible [12, 13] spectral regimes. Accessing optical frequency comb sources in integrated photonic platforms is of paramount importance for the translation of many of these technologies to real-world applications and devices [14]. Despite outstanding progress in that direction in the near-infrared, there is a dearth of widely tunable frequency comb sources, especially in the highly desired mid-infrared and visible spectral regimes.

Notable efforts on miniaturized mid-IR comb sources typically rely on supercontinuum generation, and/or intra-pulse difference frequency generation [15, 16]. Not only do these nonlinear processes usually require a femtosecond pump as an input (which has its own challenges for efficient on-chip manifestation), but their power is also distributed over a wide frequency range including undesired spectral bands. Engineered semiconductor devices like quantum cascade lasers have successfully been demonstrated as mid-infrared frequency comb sources [17], however, they are not tunable over a broad wavelength range and are still difficult to operate in the ultrashort pulse regime [18, 19]. The situation is exacerbated by the lack of a suitable laser gain medium that is amenable to room temperature operation in the mid-IR. Kerr nonlinearity can lead to tunable broadband radiation [20–22] but is contingent on satisfying demanding resonator quality

factor requirements and typically relies on a mid-IR pump to begin with for subsequent mid-infrared frequency comb generation. Similar challenges exist for Raman-based mid-IR frequency comb generation [23].

On the other hand, optical parametric oscillators (OPOs) based on quadratic nonlinearity have been the predominant way of accessing tunable coherent radiation in the mid-IR spectral region enjoying broadband tunability through appropriate phase matching of the three-wave mixing [11]. However, their impressive generation of tunable frequency combs in the mid-infrared have been limited to bulky free-space configurations pumped by femtosecond lasers [24, 25]. Recently, integrated quadratic OPOs are realized in the near-IR, using high-Q resonators with pump-resonant designs [26–28], which have not been able to access the broad tunability of phase matching and mid-IR frequency comb generation.

In this work, we demonstrate ultra-widely tunable frequency comb generation from on-chip OPOs in lithium niobate nanophotonics. Leveraging the ability to control the phase-matching via periodic poling combined with dispersion engineering, we show an on-chip tuning range that exceeds an octave. We pump the OPOs with picosecond pulses from an electro-optic frequency comb source in the near-IR, which is already demonstrated to be compatible with nanophotonic lithium niobate [29–31]. The demonstrated frequency combs cover the typical communication bands and extend into the mid-infrared spectral region beyond $3\ \mu\text{m}$ with instantaneous bandwidths supporting sub-picosecond pulse durations. Additionally, the same chip produces tunable frequency combs in the visible resulting from up-conversion processes. Tunable visible frequency comb

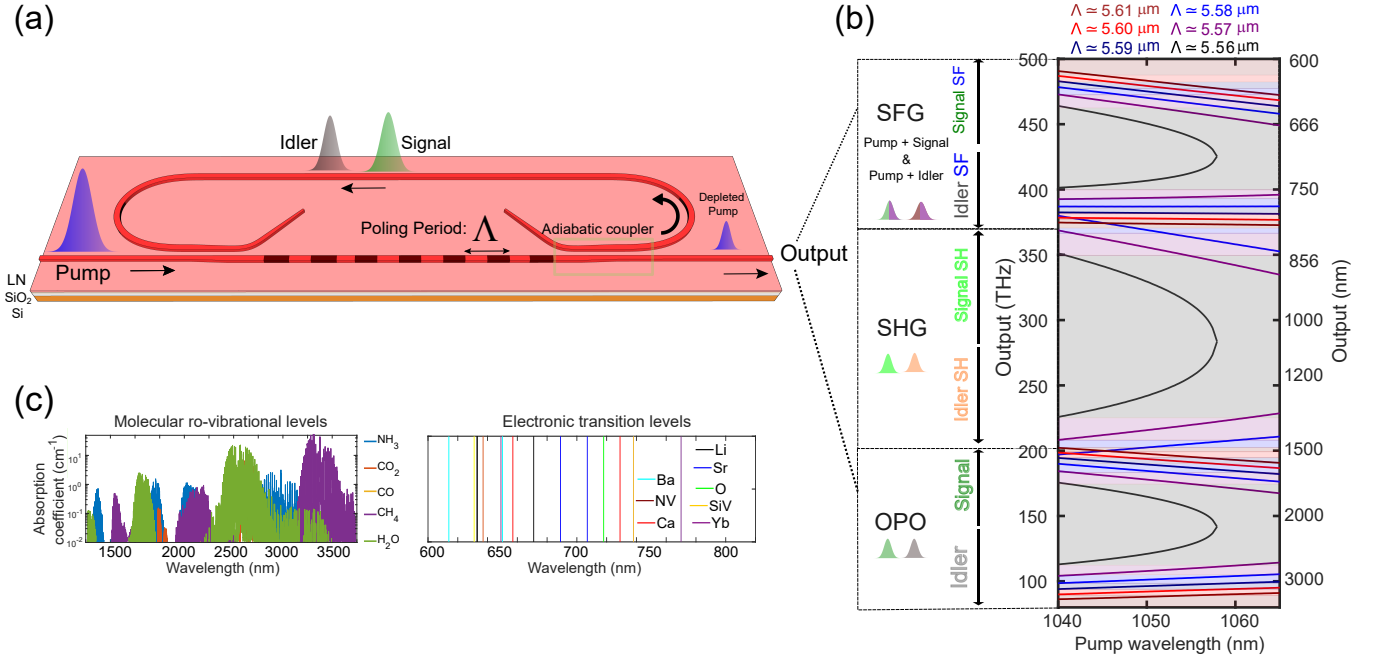


FIG. 1. **Ultra-widely tunable frequency combs from nanophotonic parametric oscillators.** a) Schematic of a doubly resonant optical parametric oscillator fabricated on an X-cut thin-film lithium niobate consisting of a periodically poled region for efficient parametric nonlinear interaction. The waveguides (dimensions: width of $2.5 \mu\text{m}$, etch depth of 250 nm) support guided-modes in the mid-infrared corresponding to the idler wave. b) Quasi-phase matched parametric gain tuning from visible-to-mid-IR. Phase-matching curves leading to tunable mid-infrared idler emission enabled by optical parametric oscillator devices with slightly different poling periods (Λ) integrated on the same chip. The same chip is capable of producing tunable visible frequency combs thanks to the sum frequency generation (SFG) process between the pump with the signal and idler waves. Other accompanying up-conversion processes includes the second-harmonic (SH) of the signal and the idler. Some second-harmonic phase-matching curves have been omitted for better clarity. c) The emission from the chip overlaps with strong molecular absorption lines in the mid-infrared covering a spectral window important for molecular spectroscopy. The spectral coverage in the visible includes atomic transition wavelengths corresponding to commonly used trapped ions/ neutral atoms/ color centers.

realization has been challenging owing to the absence of a suitable broadband gain medium and the typical large normal dispersion at these wavelengths in most integrated photonic platforms [32, 33].

To achieve broadband and widely-tunable frequency combs, we design a doubly-resonant OPO [34–36] based on nano-waveguides etched on X-cut 700-nm-thick MgO-doped lithium niobate, which is illustrated in Fig. 1(a). Unlike the previous triply-resonant designs [26–28], our design provides access to the wide tunability of quasi-phase-matching (QPM) and avoids stringent requirements such as ensuring the resonance of the pump [37]. Doubly resonant operation is achieved through controlling the precise spectral response of the OPO resonator using two spectrally selective adiabatic couplers (highlighted in Fig. 1(a)) that only let the long wavelengths (signal and idler) to resonate in the OPO while allowing the short wavelengths (pump and up-converted light) to leave the cavity (see Supplementary section 3). This is not only important for achieving a broad tuning range for the signal and the idler, it also enables non-resonant broadband and widely tunable up-conversion into the visible, which is in stark

contrast with previous parametric sources in that range [32, 33]. Another important aspect of the on-chip OPO design is the dispersion engineering of the main interaction waveguide of the OPO, which in combination with periodic poling leads to broad spectral coverage of the QPM tuning. Engineering the dispersion of the remainder of the resonator is another important design degree of freedom that can be further utilized for achieving quadratic solitons and pulse compression mechanisms [38].

Quadratic parametric nonlinear interactions take place in a 5-mm-long poled waveguide region, which has a fixed poling period (Λ) for each OPO on the chip. The periodic poling phase-matches parametric nonlinear interaction between the pump, the signal, and the idler waves which can be tuned from degeneracy to far non-degeneracy. The chip consists of multiple OPOs with poling periods for type-0 phase matching of down-conversion of a non-resonant pump at around $1 \mu\text{m}$ to an octave-spanning range of resonant signal and idler wavelengths, i.e., the OPO output. The QPM tuning curves are shown in Fig. 1(b). In addition to these OPO outputs, the poled waveguide also provides additional parametric up-

conversion processes, notably the second-harmonic of the signal/idler, and the sum-frequency generation from the pump and signal/idler. The overall tuning range of the chip overlaps with many molecular and atomic transitions as illustrated in Fig. 1(c). The strong spatio-temporal confinement of the interacting waves in the waveguide guarantees substantial up-conversion efficiencies which can be further enhanced with the addition of proper poling periods and tailoring to specific applications (see supplementary section 2).

As shown in Fig. 1(b), to continuously cover the visible to the mid-infrared, we focus on tuning the QPM by coarsely switching the poling period as well as fine-tuning the pump wavelength over ~ 25 nm. It is worth noting that this tuning range for the pump is compatible with the existing semiconductor lasers [39]. Moreover, the coarse switching of the poling period can be achieved without mechanical movements for instance by means of electro-optic routing (see supplementary section 12). In addition, temperature tuning of the poled region can provide another substantial tuning mechanism (see supplementary section 13). The emission from the OPO chip covers important wavelengths corresponding to atomic transitions in the visible as well as molecular absorption lines in the mid-infrared (Fig. 1(c)).

The OPO is synchronously pumped [35, 40, 41] by ~ 1 -ps-long pulses operating at a repetition rate of approximately 19 GHz. The repetition rate was tuned close to the OPO cavity free spectral range or its harmonics (see Supplementary section 6). The octave-wide tunability of the parametric oscillation from the OPO chip is obtained by tuning the pump central wavelength between 1040 nm and 1065 nm only. The pump is generated from an electro-optic frequency comb [42] (see Supplementary section 4). The schematic of the experimental setup is shown in Fig. 2(a). The spectral and temporal characteristics of the near-infrared pump are shown in Fig. 2(b).

Figure 2(c) shows the broad spectral coverage of the OPO output extending up to $3.3 \mu\text{m}$ in the mid-infrared obtained from a single chip. The comb lines can be resolved by the optical spectrum analyzer (OSA) and can be seen in the inset, where the separation of the peaks corresponds to the pump repetition rate. The on-chip threshold amounts to approximately 1 mW of average power (~ 50 mW of peak power, and ~ 100 femtojoules of pulse energy) for the near-degenerate OPOs. The signal conversion efficiency approaches $\sim 5\%$ for the near-degenerate OPOs, while the mid-infrared ($3.3 \mu\text{m}$) idler conversion efficiency exceeds 1% for the far non-degenerate OPOs (see Supplementary section 3). This corresponds to an estimated ~ 25 mW of peak-power and $\sim 5 \mu\text{W}$ of power per comb line in the mid-infrared (see Supplementary section 3).

The doubly-resonant operation of the OPO is also confirmed by the appearance of the resonance peak structure with the variation of the pump central wavelength as shown in Fig. 3(a). Figure 3(b) shows

the tolerance of the synchronous pumping repetition rate mismatch with respect to the optimum OPO operating point. The fine tunability of the OPO output spectra as offered by tuning the pump wavelength is depicted in Fig. 3(c). The combination of fine tunability and course tunability potentially enables continuous spectral coverage across the accessible spectral region. The OPO output at degeneracy (Fig. 3(d)) corresponds to a sub-picosecond transform-limited temporal duration (~ 400 fs), representing a pulse compression factor exceeding 2 with respect to the pump (see Supplementary section 9). We further evaluate the coherence of the output frequency comb by performing a linear field cross-correlation of the output signal light as shown in Fig. 3(e), where each OPO pulse is interfered with another pulse delayed by 10 roundtrips. The presence of the interference fringes (see inset of Fig. 3(e)), combined with the consistency of the Fourier transform of the cross-correlation trace and the signal spectrum obtained using an OSA, serve as evidence for the coherence of the output frequency comb over the entire spectrum (see Fig. 3(f)).

The occurrence of other quadratic nonlinear processes, namely second harmonic generation (SHG) and sum-frequency generation (SFG), leads to frequency comb formation in the visible spectral region. The complete emission spectrum of an OPO consisting of the second harmonic of the pump and the signal waves, the sum frequency components between the pump and the signal/idler waves along with the usual signal/idler is shown in Fig. 4(a). The scattered visible light emanated from the chip is captured by the optical microscope image (see Fig. 4(b)) showing the emission of pump second harmonic (green) and the sum frequency components (red). Note that in the poling region, green dominates at the input side, which progressively is overpowered by the sum-frequency red component. The SFG between the pump and the signal waves leads to tunable visible frequency comb generation between 600 nm and 700 nm as shown in Fig. 4(c). Tuning the OPO farther from degeneracy leads to idler emission further into the mid-IR as well as SFG component that lies to the bluer side of the visible spectrum.

The pump, which is a near-IR electro-optic comb, can be incorporated into the lithium niobate chip in the future [29, 43]. With proper dispersion engineering, our OPO design can additionally achieve large instantaneous bandwidth accompanied by significant pulse compression [38], enabling the generation of femtosecond mid-infrared frequency combs in nanophotonics. Efficient supercontinuum generation requiring only a couple of picojoules of pulse energy can then be performed using periodically-poled lithium niobate waveguides on these femtosecond pulses for subsequent f-2f self-referencing/comb stabilization [44]. Future work will involve the integration of electro-optic modulators for active locking of the OPO frequency comb. In the absence of any active feedback, the OPO output power remains stable for a long time in the laboratory

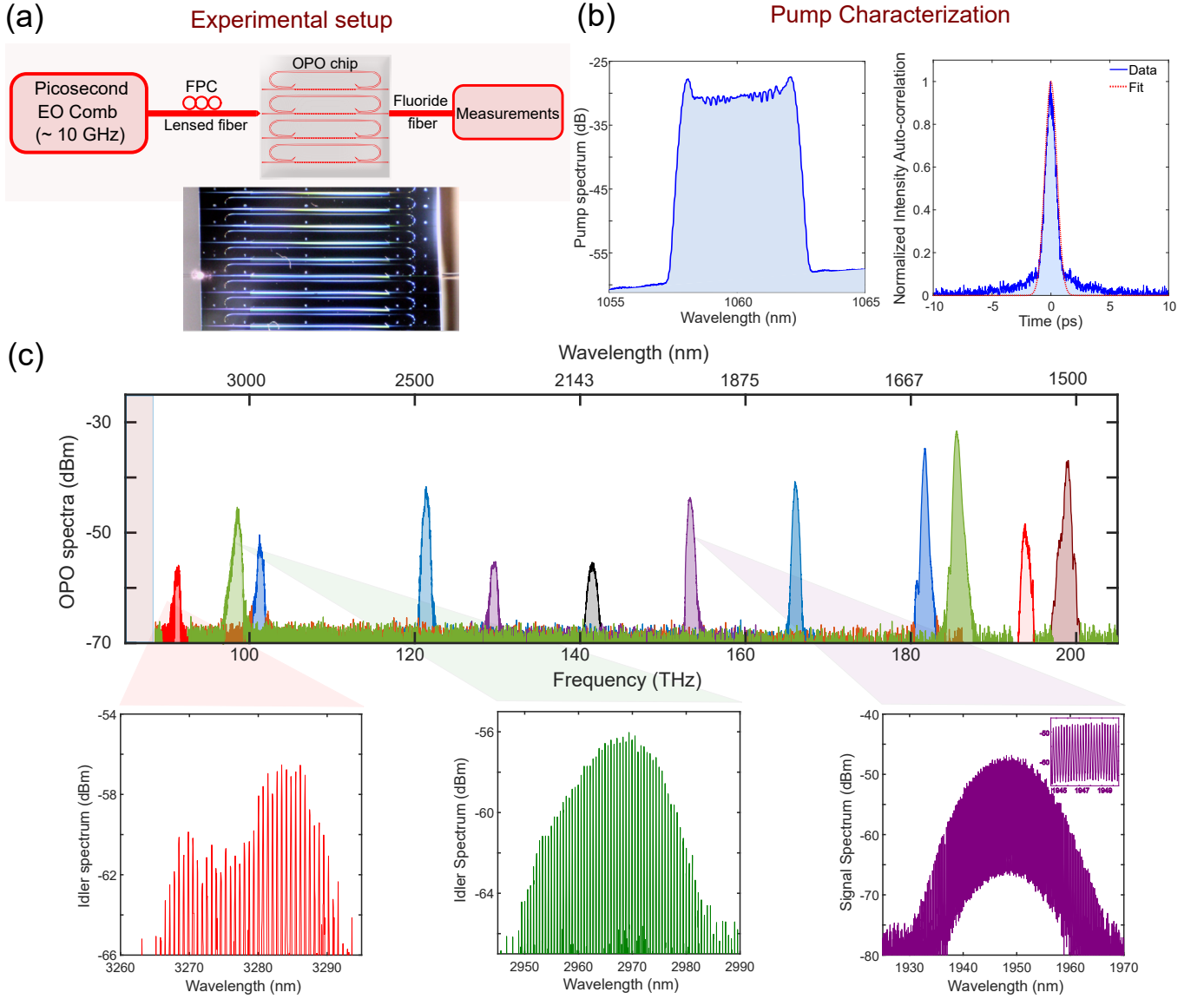


FIG. 2. Near-IR to mid-IR frequency combs from nanophotonic OPOs on a single chip. a) Schematic of the experimental setup used to pump and measure the synchronously pumped optical parametric oscillator chip. The image of the OPO chip is shown alongside, b) Experimental measurements of the spectral and temporal characteristics (intensity auto-correlation trace) of the electro-optic pulsed pump showing a pulse-width of ~ 1 ps, c) Broadband infrared spectral coverage of the OPO chip showing the signal and the idler spectrum as it's operation is tuned from degeneracy to far non-degeneracy. Separate colors represent outputs from different OPO devices on the same chip with distinct poling periods. Zoomed-in versions display the comb line structure.

environment (see Supplementary section 7). The on-chip OPO threshold can be reduced further by improving waveguide losses and enhancing the effective nonlinear co-efficient by separately optimizing the modal overlap between the pump and the signal/idler fields for each OPO device catering to dedicated spectral bands. We estimate that an on-chip threshold for operation near degeneracy with an average power less than $500 \mu\text{W}$ (for 10 GHz repetition rate operation) is feasible. The low power requirement combined with the need for a relatively narrow pump tunability range opens the

door for pumping the OPO chip with butt-coupled near-infrared diode lasers. This paves the way for a fully integrated solution for mid-IR frequency comb generation based on lithium niobate nanophotonics [30, 31, 45, 46] (see supplementary section 12).

Optimizing the coupler design can enable OPO operation with lower thresholds and higher mid-infrared comb conversion efficiency. Advanced coupler designs like the ones inspired by inverse design [47] can satisfy the simultaneous requirements of low coupling for

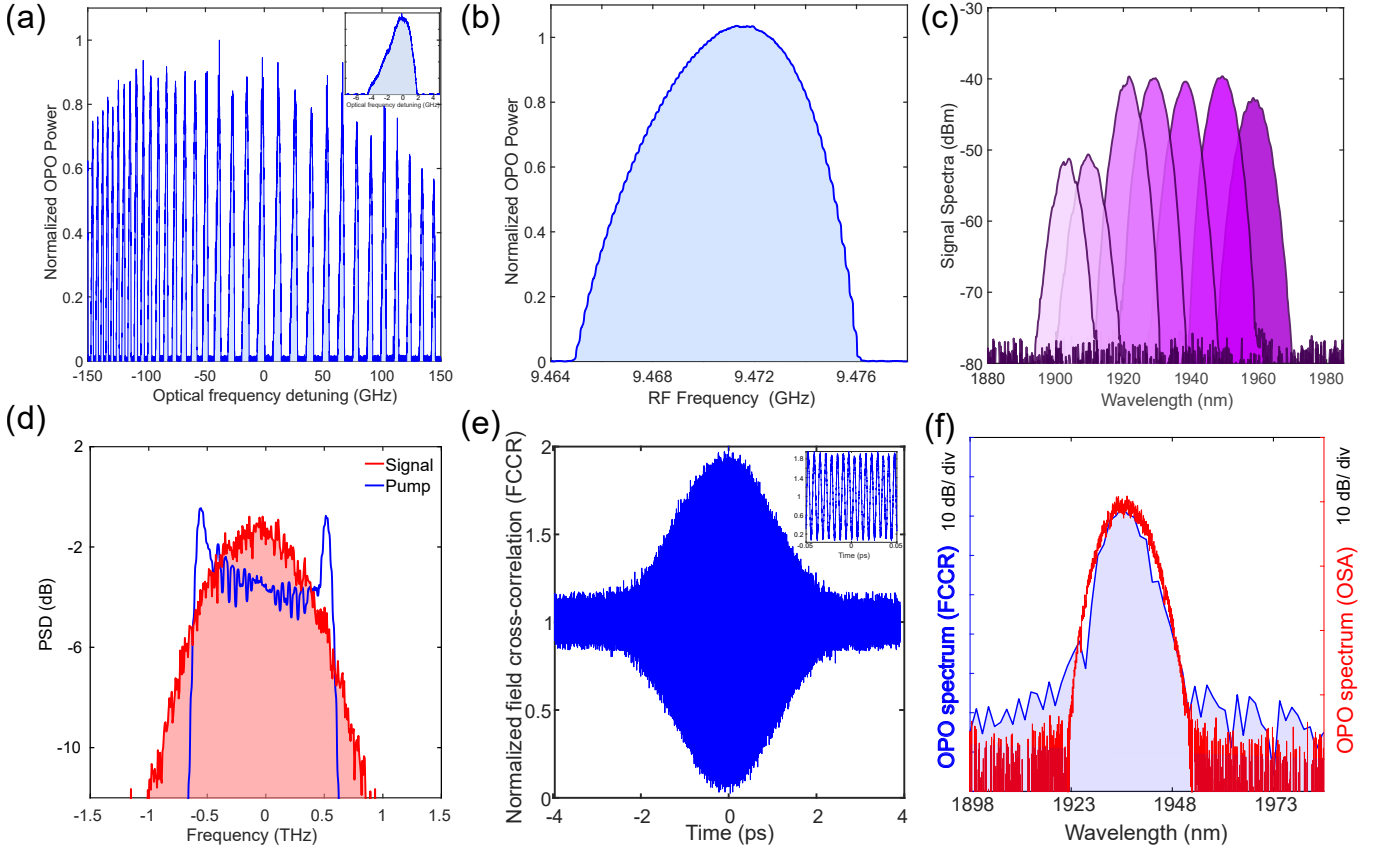


FIG. 3. **Characteristics of the frequency comb generated from the synchronously pumped on-chip OPOs.** a) Resonance peak structure obtained by sweeping the pump central wavelength which is typical of doubly-resonant OPO operation. A zoomed-in view of a single peak is shown in the inset, b) Range of existence of the synchronously pumped OPO for a fixed pump power as the pump repetition rate is varied, c) Fine tuning of the OPO frequency comb output enabled by tuning the pump central wavelength, d) Spectral broadening of the OPO operating at degeneracy corresponding to a sub-picosecond transform limited duration of ~ 400 fs, e) Verification of the coherence of the OPO output as evident from the existence of interference fringes (see inset) in the electric-field cross-correlation trace, f) The close agreement between the spectra obtained from an optical spectrum analyzer measurement and that obtained by Fourier transforming the field cross-correlation corroborates the coherence of the OPO output.

the pump, high coupling for the signal, and optimum coupling for the idler waves, leading to conversion efficiencies even exceeding 30 %. Realizing OPO devices in lithium niobate on sapphire will give access to a wider transparency window, leading to frequency comb generation deeper into the mid-infrared [48]. Thanks to the strong parametric nonlinear interaction, it is possible to realize frequency combs with lower repetition rates (~ 1 GHz) using spiral waveguides [49] in the feedback arm of the OPO resonator which will be useful for on-chip dual-comb spectroscopy applications. The emission in the mid-infrared overlaps with important molecular rovibrational absorption lines and paves the way for novel integrated spectroscopic solutions (see Supplementary section 8).

In summary, we have demonstrated widely tunable frequency combs covering from the mid-infrared (up to $3.3 \mu\text{m}$) to the visible (620 nm) using nanophotonic

OPOs on a single chip. We have shown broadband operation (supporting sub-picosecond pulses) of the OPOs at an electronically congenial repetition rate of ~ 19 GHz. The signal/idler outputs of the OPOs cover an octave of tuning (from $1.5 \mu\text{m}$ to $3.3 \mu\text{m}$) enabled by tuning the QPM. The same chip is also capable of generating tunable visible frequency combs owing to the simultaneous occurrence of several ($\chi^{(2)}$) up-conversion processes, giving access to the nearly-continuous tuning of frequency combs from visible to mid-IR.

I. METHODS

A. Device Fabrication

The devices are fabricated on a 700 nm thick X-cut MgO-doped lithium niobate on silica die (NANOLN).

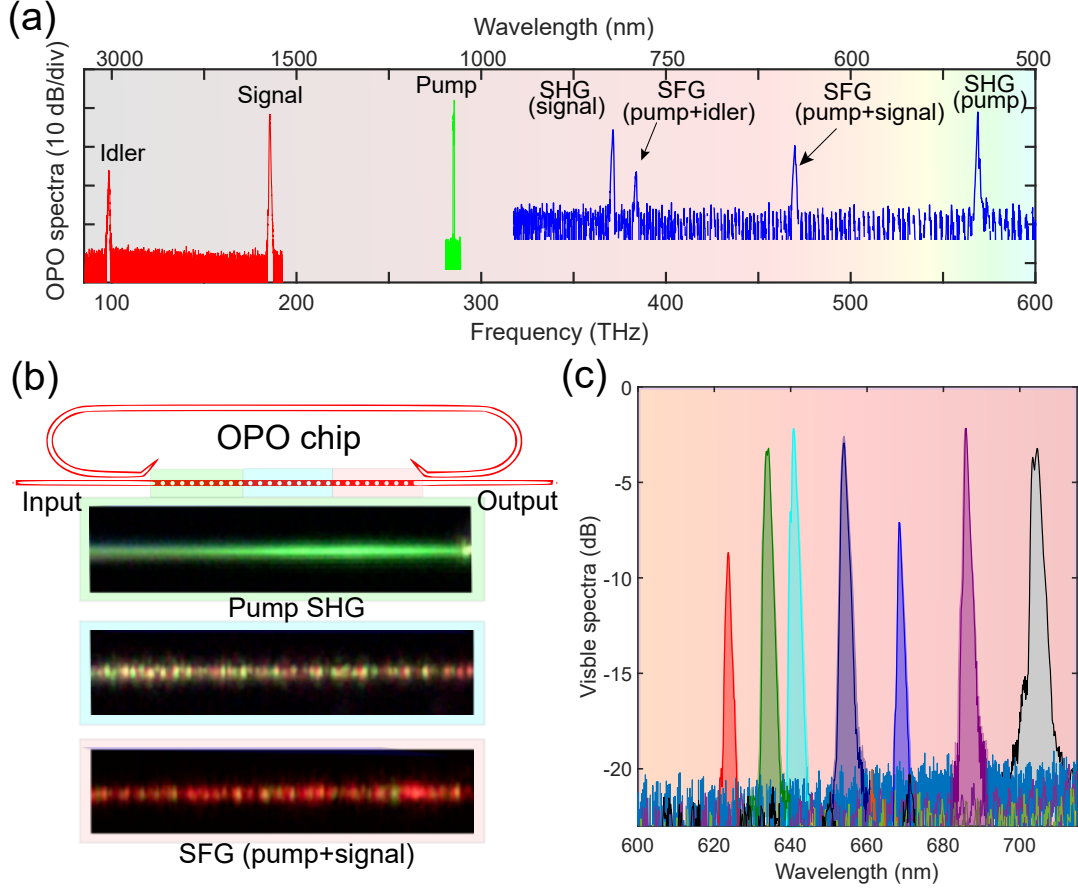


FIG. 4. **Visible frequency comb generation from the integrated optical parametric oscillator chip.** a) The complete emission spectrum of an OPO (Spectra obtained from different optical spectrum analyzers/ spectrometers are stitched together). Apart from the emission of the signal and the idler waves, the OPO also produces output in the visible spectra owing to the auxiliary nonlinear processes namely the second-harmonic generation (SHG) and the sum-frequency generation (SFG). b) Optical microscope image capturing the visible light emission from various regions of the periodically poled section of the OPO device, c) Tunable visible frequency comb generation from the integrated OPO chip, where different colors indicate spectra obtained from OPOs with distinct poling periods.

Periodic poling is performed by first patterning electrodes using e-beam lithography, followed by e-beam evaporation of Cr/ Au, and subsequently metal lift-off. Ferro-electric domain inversion is undergone by applying high voltage pulses, and the poling quality is inspected using second-harmonic microscopy. The waveguides are patterned by e-beam lithography and dry-etched with Ar^+ plasma. The waveguide facets are polished using fiber polishing films. The OPO-chip consists of multiple devices with poling periods ranging from $5.55 \mu\text{m}$ to $5.7 \mu\text{m}$ (in 10-nm increments) that provides parametric gain spanning over an octave.

B. Experimental Setup and Measurements

The simplified experimental schematic is shown in Fig 2.a, a detailed description of which is provided in supplementary sections 4, 5, and 6.

Techniques for detecting the carrier envelope offset frequencies and verifying the coherence of the OPO frequency comb are described in supplementary section 10 and 11 respectively. Optical spectra were recorded using a combination of near-infrared optical spectrum analyzer (OSA) (Yokogawa AQ6374), mid-infrared OSAs (Yokogawa AQ6375B, AQ6376E), and a CCD spectrometer (Thorlabs CCS200). The OPOs are synchronously driven at either the fundamental repetition rate ($\sim 9.5 \text{ GHz}$) or its harmonic ($\sim 19 \text{ GHz}$). The optical spectrum results are obtained with the harmonic repetition rate operation as it leads to wider instantaneous bandwidth owing to shorter electro-optic pump pulses. The OPOs operating at longer wavelengths have higher thresholds (because of increased effective area, increased coupler loss corresponding to the signal wave, and larger mismatch between the relative walk-off parameters of the signal and the idler wave) and therefore, we operate them intermittently in what we

call “quasi-synchronous” operation, as a way to reduce the average power and avoid thermal damage. (see Supplementary section 5). This limitation is mainly attributed to the avoidable input insertion loss (~ 12 dB) of our current setup. With the aid of better fiber-to-chip coupling design/mechanisms (insertion loss of the order of 1 dB has been reported in the context of thin-film lithium niobate) the mid-IR OPOs can be operated in a steady state sync-pumped configuration [50].

C. System Modeling and Simulation

We used commercial software (Ansys Lumerical) to solve for the waveguide modes, obtain the tuning/phase-matching curves, as well as to design the adiabatic coupler. For the nonlinear optical simulation, we simulated both the dual envelope model (supplementary

section 1) and the single envelope model (supplementary section 2) using the split-step Fourier algorithm.

II. DATA AVAILABILITY

The data that support the plots within this paper and other findings of this study are available from the corresponding author upon reasonable request.

III. CODE AVAILABILITY

The codes that support the findings of this study are available from the corresponding author upon reasonable request.

-
- [1] Scott A Diddams, Kerry Vahala, and Thomas Udem. Optical frequency combs: Coherently uniting the electromagnetic spectrum. *Science*, 369(6501):eaay3676, 2020.
 - [2] Tobias J Kippenberg, Alexander L Gaeta, Michal Lipson, and Michael L Gorodetsky. Dissipative kerr solitons in optical microresonators. *Science*, 361(6402):eaan8083, 2018.
 - [3] Ian Coddington, Nathan Newbury, and William Swann. Dual-comb spectroscopy. *Optica*, 3(4):414–426, 2016.
 - [4] Pablo Marin-Palomo, Juned N Kemal, Maxim Karpov, Arne Kordts, Joerg Pfeifle, Martin HP Pfeiffer, Philipp Trocha, Stefan Wolf, Victor Brasch, Miles H Anderson, et al. Microresonator-based solitons for massively parallel coherent optical communications. *Nature*, 546(7657):274–279, 2017.
 - [5] Xingyuan Xu, Mengxi Tan, Bill Corcoran, Jiayang Wu, Andreas Boes, Thach G Nguyen, Sai T Chu, Brent E Little, Damien G Hicks, Roberto Morandotti, et al. 11 tops photonic convolutional accelerator for optical neural networks. *Nature*, 589(7840):44–51, 2021.
 - [6] Liron Stern, Jordan R Stone, Songbai Kang, Daniel C Cole, Myoung-Gyun Suh, Connor Fredrick, Zachary Newman, Kerry Vahala, John Kitching, Scott A Diddams, et al. Direct kerr frequency comb atomic spectroscopy and stabilization. *Science advances*, 6(9):eaax6230, 2020.
 - [7] Myoung-Gyun Suh and Kerry J Vahala. Soliton microcomb range measurement. *Science*, 359(6378):884–887, 2018.
 - [8] Philipp Trocha, M Karpov, D Ganin, Martin HP Pfeiffer, Arne Kordts, S Wolf, J Krockenberger, Pablo Marin-Palomo, Claudius Weimann, Sebastian Randel, et al. Ultrafast optical ranging using microresonator soliton frequency combs. *Science*, 359(6378):887–891, 2018.
 - [9] Xingchen Ji, Xinwen Yao, Alexander Klenner, Yu Gan, Alexander L Gaeta, Christine P Hendon, and Michal Lipson. Chip-based frequency comb sources for optical coherence tomography. *Optics express*, 27(14):19896–19905, 2019.
 - [10] Albert Schliesser, Nathalie Picqué, and Theodor W Hänsch. Mid-infrared frequency combs. *Nature photonics*, 6(7):440–449, 2012.
 - [11] Majid Ebrahim-Zadeh and Irina T Sorokina. *Mid-infrared coherent sources and applications*. Springer Science & Business Media, 2007.
 - [12] Myoung-Gyun Suh, Xu Yi, Yu-Hung Lai, S Leifer, Ivan S Grudin, G Vasisht, Emily C Martin, Michael P Fitzgerald, G Doppmann, J Wang, et al. Searching for exoplanets using a microresonator astrocomb. *Nature photonics*, 13(1):25–30, 2019.
 - [13] Ewelina Obrzud, Monica Rainer, Avet Harutyunyan, Miles H Anderson, Junqiu Liu, Michael Geiselmann, Bruno Chazelas, Stefan Kundermann, Steve Lecomte, Massimo Cecconi, et al. A microphotonic astrocomb. *Nature Photonics*, 13(1):31–35, 2019.
 - [14] Brian Stern, Xingchen Ji, Yoshitomo Okawachi, Alexander L Gaeta, and Michal Lipson. Battery-operated integrated frequency comb generator. *Nature*, 562(7727):401–405, 2018.
 - [15] Hairun Guo, Clemens Herkommer, Adrien Billat, Davide Grassani, Chuankun Zhang, Martin HP Pfeiffer, Wenle Weng, Camille-Sophie Bres, and Tobias J Kippenberg. Mid-infrared frequency comb via coherent dispersive wave generation in silicon nitride nanophotonic waveguides. *Nature Photonics*, 12(6):330–335, 2018.
 - [16] Abijith S Kowligy, David R Carlson, Daniel D Hickstein, Henry Timmers, Alexander J Lind, Peter G Schunemann, Scott B Papp, and Scott A Diddams. Mid-infrared frequency combs at 10 ghz. *Optics Letters*, 45(13):3677–3680, 2020.
 - [17] Andreas Hugi, Gustavo Villares, Stéphane Blaser, HC Liu, and Jérôme Faist. Mid-infrared frequency comb based on a quantum cascade laser. *Nature*, 492(7428):229–233, 2012.
 - [18] Yu Yao, Anthony J Hoffman, and Claire F Gmachl. Mid-infrared quantum cascade lasers. *Nature Photonics*, 6(7):432–439, 2012.

- [19] Christine Y Wang, Lyuba Kuznetsova, VM Gkortsas, Laurent Diehl, Franz X Kaertner, Mikhail A Belkin, Alexey Belyanin, Xiaofeng Li, Donhee Ham, Harald Schneider, et al. Mode-locked pulses from mid-infrared quantum cascade lasers. *Optics Express*, 17(15):12929–12943, 2009.
- [20] Anatoliy A Savchenkov, Vladimir S Ilchenko, Fabio Di Teodoro, Paul M Belden, William T Lotshaw, Andrey B Matsko, and Lute Maleki. Generation of kerr combs centered at 4.5 μm in crystalline microresonators pumped with quantum-cascade lasers. *Optics letters*, 40(15):3468–3471, 2015.
- [21] Mengjie Yu, Yoshitomo Okawachi, Austin G Griffith, Michal Lipson, and Alexander L Gaeta. Mode-locked mid-infrared frequency combs in a silicon microresonator. *Optica*, 3(8):854–860, 2016.
- [22] Austin G Griffith, Ryan KW Lau, Jaime Cardenas, Yoshitomo Okawachi, Aseema Mohanty, Romy Fain, Yoon Ho Daniel Lee, Mengjie Yu, Christopher T Phare, Carl B Poitras, et al. Silicon-chip mid-infrared frequency comb generation. *Nature communications*, 6(1):1–5, 2015.
- [23] Yuxing Tang, Logan G Wright, Kriti Charan, Tianyu Wang, Chris Xu, and Frank W Wise. Generation of intense 100 fs solitons tunable from 2 to 4.3 μm in fluoride fiber. *Optica*, 3(9):948–951, 2016.
- [24] Florian Adler, Kevin C Cossel, Michael J Thorpe, Ingmar Hartl, Martin E Fermann, and Jun Ye. Phase-stabilized, 1.5 w frequency comb at 2.8–4.8 μm . *Optics letters*, 34(9):1330–1332, 2009.
- [25] Luke Maidment, Peter G Schunemann, and Derryck T Reid. Molecular fingerprint-region spectroscopy from 5 to 12 μm using an orientation-patterned gallium phosphide optical parametric oscillator. *Optics Letters*, 41(18):4261–4264, 2016.
- [26] Juanjuan Lu, Ayed Al Sayem, Zheng Gong, Joshua B Surya, Chang-Ling Zou, and Hong X Tang. Ultralow-threshold thin-film lithium niobate optical parametric oscillator. *Optica*, 8(4):539–544, 2021.
- [27] Yang He, Qi-Fan Yang, Jingwei Ling, Rui Luo, Hanxiao Liang, Mingxiao Li, Boqiang Shen, Heming Wang, Kerry Vahala, and Qiang Lin. Self-starting bi-chromatic linbo 3 soliton microcomb. *Optica*, 6(9):1138–1144, 2019.
- [28] Alexander W Bruch, Xianwen Liu, Zheng Gong, Joshua B Surya, Ming Li, Chang-Ling Zou, and Hong X Tang. Pockels soliton microcomb. *Nature Photonics*, 15(1):21–27, 2021.
- [29] Mian Zhang, Brandon Buscaino, Cheng Wang, Amirhassan Shams-Ansari, Christian Reimer, Rongrong Zhu, Joseph M Kahn, and Marko Lončar. Broadband electro-optic frequency comb generation in a lithium niobate microring resonator. *Nature*, 568(7752):373–377, 2019.
- [30] Mengjie Yu, Christian Reimer, David Barton, Prashanta Kharel, Rebecca Cheng, Lingyan He, Linbo Shao, Di Zhu, Yaowen Hu, Hannah R Grant, et al. Femtosecond pulse generation via an integrated electro-optic time lens. *arXiv preprint arXiv:2112.09204*, 2021.
- [31] Yaowen Hu, Mengjie Yu, Brandon Buscaino, Neil Sinclair, Di Zhu, Rebecca Cheng, Amirhassan Shams-Ansari, Linbo Shao, Mian Zhang, Joseph M Kahn, et al. High-efficiency and broadband on-chip electro-optic frequency comb generators. *Nature Photonics*, 16(10):679–685, 2022.
- [32] Xiyuan Lu, Gregory Moille, Ashutosh Rao, Daron A Westly, and Kartik Srinivasan. On-chip optical parametric oscillation into the visible: generating red, orange, yellow, and green from a near-infrared pump. *Optica*, 7(10):1417–1425, 2020.
- [33] Xiang Guo, Chang-Ling Zou, Hojoong Jung, Zheng Gong, Alexander Bruch, Liang Jiang, and Hong X. Tang. Efficient generation of a near-visible frequency comb via cherenkov-like radiation from a kerr microcomb. *Phys. Rev. Applied*, 10:014012, Jul 2018.
- [34] Ryan Hamerly, Alireza Marandi, Marc Jankowski, Martin M Fejer, Yoshihisa Yamamoto, and Hideo Mabuchi. Reduced models and design principles for half-harmonic generation in synchronously pumped optical parametric oscillators. *Physical Review A*, 94(6):063809, 2016.
- [35] Arkadev Roy, Saman Jahani, Carsten Langrock, Martin Fejer, and Alireza Marandi. Spectral phase transitions in optical parametric oscillators. *Nature communications*, 12(1):1–9, 2021.
- [36] Luis Ledezma, Arkadev Roy, Luis Costa, Ryoto Sekine, Robert Gray, Qiushi Guo, Ryan M Briggs, and Alireza Marandi. Widely-tunable optical parametric oscillator in lithium niobate nanophotonics. *arXiv preprint arXiv:2203.11482*, 2022.
- [37] Robert C Eckardt, CD Nabors, William J Kozlovsky, and Robert L Byer. Optical parametric oscillator frequency tuning and control. *JOSA B*, 8(3):646–667, 1991.
- [38] Arkadev Roy, Rajveer Nehra, Saman Jahani, Luis Ledezma, Carsten Langrock, Martin Fejer, and Alireza Marandi. Temporal walk-off induced dissipative quadratic solitons. *Nature Photonics*, 16(2):162–168, 2022.
- [39] Paul A Verrinder, Lei Wang, Joseph Fridlander, Fengqiao Sang, Victoria Rosborough, Michael Nickerson, Guangning Yang, Mark Stephen, Larry Coldren, and Jonathan Klamkin. Gallium arsenide photonic integrated circuit platform for tunable laser applications. *IEEE Journal of Selected Topics in Quantum Electronics*, 28(1):1–9, 2021.
- [40] Ewelina Obrzud, Steve Lecomte, and Tobias Herr. Temporal solitons in microresonators driven by optical pulses. *Nature Photonics*, 11(9):600–607, 2017.
- [41] Jiang Li, Chengying Bao, Qing-Xin Ji, Heming Wang, Lue Wu, Stephanie Leifer, Charles Beichman, and Kerry Vahala. Efficiency of pulse pumped soliton microcombs. *Optica*, 9(2):231–239, 2022.
- [42] Alexandre Parriaux, Kamal Hammani, and Guy Millot. Electro-optic frequency combs. *Advances in Optics and Photonics*, 12(1):223–287, 2020.
- [43] Camiel Op de Beeck, Felix M Mayor, Stijn Cuyvers, Stijn Poelman, Jason F Herrmann, Okan Atalar, Timothy P McKenna, Bahawal Haq, Wentao Jiang, Jeremy D Witmer, et al. Iii/v-on-lithium niobate amplifiers and lasers. *Optica*, 8(10):1288–1289, 2021.
- [44] Marc Jankowski, Carsten Langrock, Boris Desiatov, Alireza Marandi, Cheng Wang, Mian Zhang, Christopher R Phillips, Marko Lončar, and MM Fejer. Ultrabroadband nonlinear optics in nanophotonic periodically poled lithium niobate waveguides. *Optica*, 7(1):40–46, 2020.
- [45] Luis Ledezma, Ryoto Sekine, Qiushi Guo, Rajveer Nehra, Saman Jahani, and Alireza Marandi. Intense optical parametric amplification in dispersion-engineered

- nanophotonic lithium niobate waveguides. *Optica*, 9(3):303–308, 2022.
- [46] Qiushi Guo, Ryoto Sekine, Luis Ledezma, Rajveer Nehra, Devin J Dean, Arkadev Roy, Robert M Gray, Saman Jahani, and Alireza Marandi. Femtojoule femtosecond all-optical switching in lithium niobate nanophotonics. *Nature Photonics*, 16(9):625–631, 2022.
 - [47] Sean Molesky, Zin Lin, Alexander Y Piggott, Weiliang Jin, Jelena Vucković, and Alejandro W Rodriguez. Inverse design in nanophotonics. *Nature Photonics*, 12(11):659–670, 2018.
 - [48] Jatadhari Mishra, Timothy P McKenna, Edwin Ng, Hubert S Stokowski, Marc Jankowski, Carsten Langrock, David Heydari, Hideo Mabuchi, MM Fejer, and Amir H Safavi-Naeini. Mid-infrared nonlinear optics in thin-film lithium niobate on sapphire. *Optica*, 8(6):921–924, 2021.
 - [49] Hansuek Lee, Tong Chen, Jiang Li, Oskar Painter, and Kerry J Vahala. Ultra-low-loss optical delay line on a silicon chip. *Nature communications*, 3(1):1–7, 2012.
 - [50] Changran Hu, An Pan, Tingan Li, Xuanhao Wang, Yuheng Liu, Shiqi Tao, Cheng Zeng, and Jinsong Xia. High-efficient coupler for thin-film lithium niobate waveguide devices. *Optics Express*, 29(4):5397–5406, 2021.

IV. ACKNOWLEDGMENTS

The device nanofabrication was performed at the Kavli Nanoscience Institute (KNI) at Caltech. This work was supported by a NASA Space Technology Graduate Research Opportunities Award. The authors thank NTT Research for their financial and technical support. The authors thank Dr. Mahmood Bagheri for loaning the Mid-IR optical spectrum analyzer. The authors gratefully acknowledge support from ARO grant no. W911NF-18-1-0285, AFOSR award FA9550-20-1-0040, NSF Grant No. 1846273, and 1918549, and NASA.

V. AUTHOR CONTRIBUTION

A.R, L.L, L.C, R.G performed the experiments. L.L fabricated the chip with help from R.S. A.R, L.L, and R.G performed the numerical simulations. All authors participated in the design, discussions, and debugging. A.R. and A.M. wrote the manuscript with input from all authors. A.M. supervised the project.

VI. COMPETING INTERESTS

L.L, R.M.B. and A.M: US patent 11,226,538 (P). The remaining authors declare no conflicts of interest.